HAYATI
Journal of Biosciences

Vol. 33 No. 3, May 2026 617-633
DOI:10.4308/hjb.33.3.617-633
ISSN: 1978-3019
EISSN: 2086-4094

Research Article

Preparation and Characterization of P(3HB-co-HHX)/Silk Fibroin Nanofiber for Chondrogenic Differentiation on Human Adipose Mesenchymal Stem Cell

Andri Pramesyanti Pramono[1*], Retno Yulianti[2], Muhamad Alif Razi[3], Karina[2], Shaik Ling Ang[4], Kumar Sudesh[4], Hanan[2], Yuni Cahya Endarwati[5], Muhammad Radian Ghoza[6]

[1]Research Center for Molecular Biology Eijkman, National Research and Innovation Agency (BRIN), Kawasan Sains Teknologi Dr. (H.C.) Ir. H. Soekarno Jl. Raya Bogor Km. 46, Cibinong 16911, Indonesia
[2]Faculty of Medicine, Universitas Pembangunan Nasional Veteran Jakarta, Pondok Labu, Depok 12450, Indonesia
[3]Faculty of Engineering, Universitas Pembangunan Nasional Veteran Jakarta, Depok 12450, Indonesia
[4]School of Biological Sciences, Universiti Sains Malaysia (USM), Penang 11800, Malaysia
[5]Department of Animal Production and Technology, Faculty of Animal Science, IPB University, Jl. Agathis Kampus IPB Dramaga, Bogor 16680, Indonesia
[6]Master's Programme in Biomedical Science, Faculty of Medicine, Universitas Indonesia, Jakarta, Indonesia

ARTICLE INFO

Article history:
Received September 22, 2025
Received in revised form November 18, 2025
Accepted November 26, 2025
Available Online January 13, 2026

KEYWORDS:
Adipose mesenchymal stem cell,
PHA-Silk,
nanofiber,
silk fibroin,
cartilage stem cell differentiation

ABSTRACT

This study explored the proliferative and chondrogenic differentiation capacities of nanofiber containing silk fibroin hybrid Bombyx mori silkworm cocoons (Japan-China SP-01 variant from Indonesia) and PHA P(3HB-co-3HHx) on human adipose mesenchymal stem cells. First, the scaffolds were prepared for electrospinning by combining two distinct biomaterials, consisting of silk fibroin derived from hybrid *Bombyx mori* silkworm cocoons, with a combination of 3-hydroxybutyrate (3HB) and 3-hydroxyhexanoate (3HHx). The effects of various ratios of P(3HB-co-3HHx)/Silk Fibroin nanofiber mixture on proliferative and differentiation capacity were then investigated. Following that, the morphology, chemical compositions, contact angle, tensile strength, roughness, cell viability, and human adipose mesenchymal stem cell differentiation of the nanofiber were investigated by collagen type 2 gene expression. The results of scanning electron microscopy showed the mean diameter of the nanofiber ranged from 370-600 nm. Following that, 16,000 volts was prominent for nanofiber manufacture in all ratios. It was also demonstrated that the nanofiber has significant mechanical properties, acceptable hydrophilicity and smoothness, and appropriate cell viability (up to 99.1% compared to the control on silk fibroin nanofiber). Although PHA increased tensile strength, silk fibroin administration to the mixture predominantly enhanced chondrogenic differentiation, as evidenced by modulation of chondrogenic collagen type 2 (up to 8.718-fold) gene markers. Furthermore, the physicochemical characteristics of the nanofiber mixture significantly influenced the proliferation and differentiation of human adipose mesenchymal stem cells. The results of the tests showed that silk fibroin administration into a nanofiber mixture has improved chondrogenesis and showed great potential as a cartilage tissue scaffold.

1. Introduction

As demand for regenerative therapies has surged, the cultivation of stem cells capable of reliably repairing damaged tissues has intensified. One of the greatest obstacles is ensuring that a sufficient number of stem cells are available and that they can multiply while retaining their unique abilities. The development of efficient scaffolds is crucial for successful stem cell therapies, as they can significantly boost cell proliferation and differentiation. (Barcena *et al.* 2024) Mesenchymal stem

*Corresponding Author
E-mail Address: andr060@brin.go.id

cells can differentiate into chondrocytes, osteocytes, and myocytes when induced inappropriately (Kangari *et al.* 2020). Adipose mesenchymal stem cells (ADSC) offer easy, abundant, and safe harvesting for autologous therapy, especially in cartilage damage-related disease, compared to other stem cell resources. This eliminates the problem of immune rejection and addresses ethical issues, as they come from the patient's own body. This strategy holds significant clinical relevance for treating cartilage-related diseases, including osteoarthritis, traumatic chondral injuries, intervertebral disc degeneration, rheumatoid arthritis–associated cartilage destruction, osteochondritis dissecans, and congenital skeletal disorders. It offers the potential for durable, biologically compatible regenerative solutions. However, the reconstruction using human adipose mesenchymal stem cell regenerative therapy also requires scaffolds that support the proliferation and differentiation (Bari *et al.* 2021). Determining the characteristics and functions of scaffolds by assessing their *in vitro* cell proliferation and differentiation capacity is critical.

Silk and polyhydroxyalkanoate (PHA) are natural polymer scaffolds with the potential to support proliferation and differentiation (Bari *et al.* 2021; Zhang *et al.* 2021; Pecorini *et al.* 2022; Kopf *et al.* 2023). A previous study showed that human umbilical cord mesenchymal stem cells (hUCMSCs) seeded on PHA/silk nanofibers could be successfully induced to undergo osteogenic differentiation. However, the application of nanofibers to human adipose mesenchymal stem cells for chondrogenic and cartilage tissue engineering, which possess different biological properties compared to umbilical cord-derived MSCs, has not yet been optimized or investigated in this context. Here, we used a different source of isolated silk fibroin compound from hybrid *Bombyx mori* silkworm cocoons, Japan-China SP-01 variant from Indonesia (Kiyosawa *et al.* 1999). This investigation employed biomarkers of chondrogenesis, namely collagen type 2, to provide an overview of biomaterials for stem cell chondrogenesis. This study aimed to investigate the proliferation and chondrogenesis differentiation capacity of ADSCs on silk and polyhydroxyalkanoate (PHA) nanofibers.

2. Materials and Methods

This research was designed as an *in vitro* experimental study to investigate five distinct weight ratios of P(3HB-co-3HHx)/silk fibroin nanofibers mixtures (4:0, 3:1, 1:1, 1:3, and 0:4), evaluating their morphology, chemical composition, contact angle, tensile strength, surface roughness, cell viability, and the differentiation capacity of human adipose mesenchymal stem cells.

2.1. Materials

PHA is a copolymer of 3-hydroxybutyrate and 3-hydroxyhexanoate [P(3HB-co-3HHx)]. It is biosynthesized by *Cupriavidus necator*. The copolymer P(3HB-co-3HHx) used in this study comprised 92 mol% 3HB and 8 mol% 3HHx-monomers (Murugan *et al.* 2017). The mesenchymal stem cells from adipose tissue were obtained from healthy patients.

2.2. PHA Polymer Isolation

PHA was extracted from freeze-dried cells of *Cupriavidus necator* by agitation and was biosynthesized through a fermentation process. Freeze-dried cells were shaken in 1:100 chloroform at room temperature for five days. Cell debris was removed by filtering the resulting solution through Whatman filter paper no. 1. The solution was concentrated by a rotary evaporator (EYELA, Japan) in a 60°C water bath. The concentrated mixture was thereafter introduced into 10 liters of vigorously stirred, cooled methanol. The mixture was allowed to remain undisturbed for several hours to facilitate PHA precipitation until the supernatant became clear. Following filtration and air-drying overnight under a fume apparatus, PHA was kept in an airtight container for further use (Murugan *et al.* 2017).

2.3. Silk Fibroin Extraction

We extracted silk fibroin from the cocoons of hybrid *Bombyx mori* silkworm cocoons (Japan-China SP-01 variant) from Indonesia. Sericin was extracted according to the method described by Ang *et al.* (2020), with some modifications (Figure 1). The silk fibroin solution was lyophilized and stored at room temperature before use (Rockwood *et al.* 2011; Ang *et al.* 2020).

2.4. Solution Preparation for Electrospinning

Five distinct weight ratios of the P(3HB-co-3HHx)/silk fibroin mixed solution were prepared by dissolving the polymer in hexafluoroisopropanol (HFIP) to a final concentration of 4% (w/v): 4:0, 3:1, 1:1, 1, 1:3, and 0:4. P(3HB-co-3HHx) and silk fibroin were completely dissolved in the polymer solution by stirring at an ambient temperature (25°C) for 48 h.

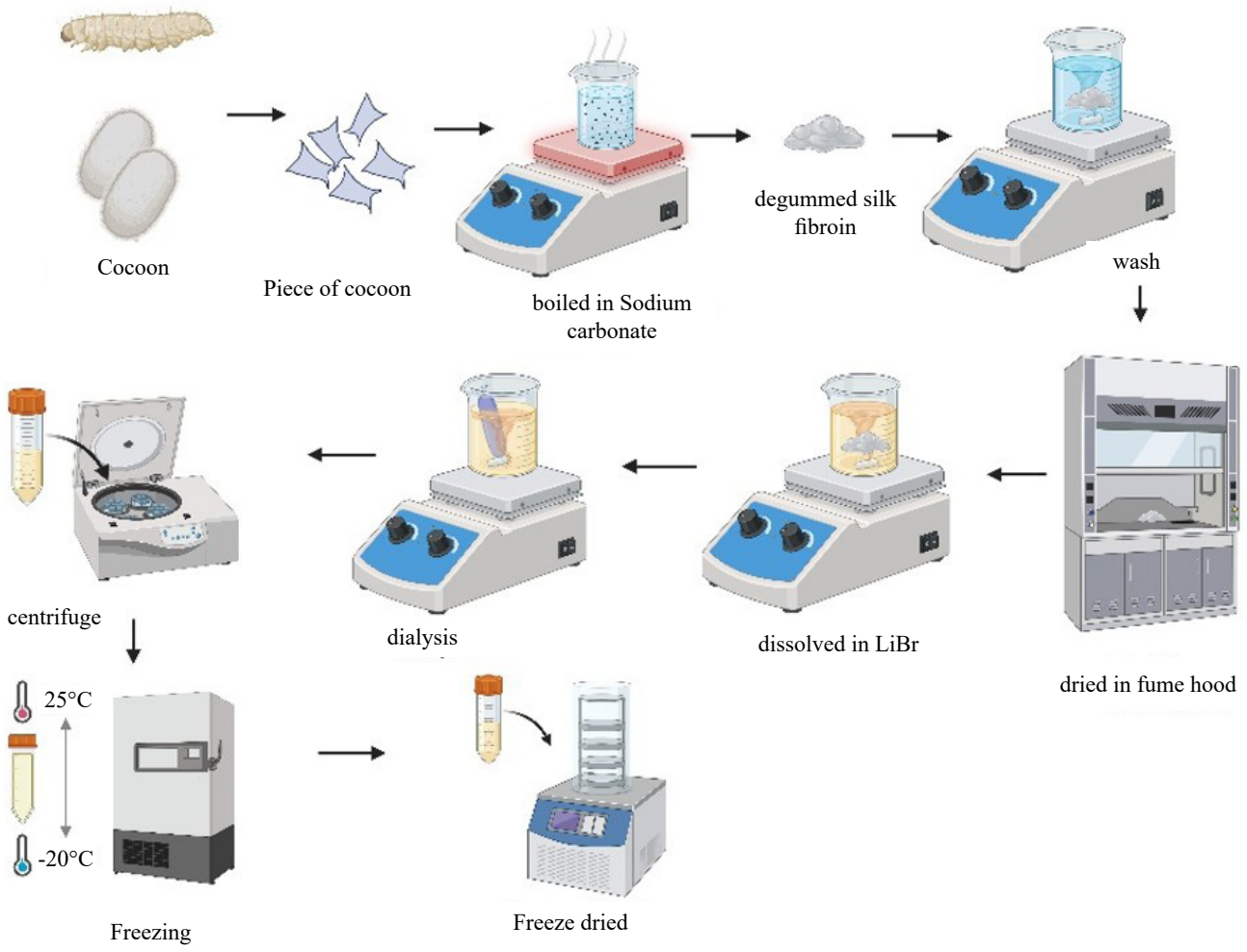

Figure 1. Illustration of silk fibroin isolation from bombyx morii cocoon (made by Biorender.com)

2.5. Electrospinning Process

Electrospinning was performed using an Esprayer ES-2000 (Fuence Co. Ltd., Japan). A 21-gauge needle was used to extrude the polymer solution using a glass syringe. During the entire procedure, the flow rate remained constant at 15 µL/min, whereas the distance between the collector and the needle point of the injector was 20 cm. Various voltages (14,000,16,000, and 18,000 volts) were applied to achieve sustained jets. All nanofibers were treated with 100% ethanol for 30 min before characterization and cell culture procedures.

2.6. Scanning Electron Microscopy (SEM)

The surface structures and morphologies of the nanofiber were investigated using SEM. Before examination using a scanning electron microscope (TM-4000, Hitachi, Japan), the nanofibers were adhered to aluminum fragments using conductive carbon. The mean and dispersion of the fiber diameters were ascertained using the ImageJ software. The results were entered in a Microsoft Excel spreadsheet. The microstructure of the PHA-Silk combination at different ratios was examined using SEM to determine if the nanofiber diameter was in the nanometer range.

2.7. Fourier Transform-infrared (FT-IR) Spectroscopy

The functional groups present in the nanofiber were characterized using a Fourier transform infrared (FT-IR) spectrometer (Frontier IR, PerkinElmer Inc., USA) with an attenuated total reflectance (ATR) accessory. All spectra of the samples were recorded in the wavenumber range of 4,000-600 cm^{-1} with a spectral resolution of 4 cm^{-1}, and the results were definitive.

2.8. Water Contact Angle

We determined the static contact angle using the sessile drop method on a nanofiber with an Attension

Theta Optical Tensiometer (Biolin Scientific, Finland). The technique for determining the contact angles was as follows: one electrospun membrane sample was adsorbed onto a glass slide, after which the contact angles were measured according to the following guidelines: a droplet of distilled water measuring 3 µL was used. Contact angle tests were performed immediately, within 15 seconds of placing a drop of distilled water on the surface of the electrospun membrane using Attension Theta software. We obtained summary statistics for each sample using the mean values of three measurements.

2.9. Atomic Force Microscope (AFM) Analysis

To observe the surface roughness of the blend nanofibers, we employed a three-dimensional topographic technique with a high atomic resolution in the form of AFM. The roughness parameters of the surfaces were determined using the AFM software, which includes additional functions for calculating the roughness parameters using Ra. The results, presented in numerous tables and graphs, offer precise insights into the surface properties of nanofibers.

2.10. Tensile Test

Morphological analysis of the electrospun membrane indicated that its mechanical interconnectivity may have been established by thinning and weakness. The points of grasp and throughout the handling process are used to mitigate cracking. Adhesive tape was affixed to the two edges of the sample as a preventative measure. Tensile tests were conducted on the samples using an Instron 3369 Universal Test Machine (United States of America), which has a load-measuring capacity of 0.0001 N. The ground portions of the samples were attached. The gripping areas of the two pneumatic jaws were approximately 0.3 mm and prepared into rectangular cross-sections with 10 mm of length left at both ends for gripping by the jaws. All samples were analysed in triplicate.

2.11. Isolation and Culture of Adipose Mesenchymal Stem Cells

Abdominal liposuction was employed to divide the panniculus adiposus, a human solid fat, into diminutive pieces measuring 1-3 mm. This was achieved by using a scalpel and forceps. Upon completion of the procedure, 10-15 mL of minced fat was transferred into a 50 mL reaction tube. The cells were subsequently cultured in a 25 cm^2 flask at 37°C using DMEM, which was supplemented with 10% fetal bovine serum and 1% penicillin/streptomycin (Gibco) containing 10,000 units/mL of penicillin and 10,000 µg/mL of streptomycin in a 5% CO_2 incubator. These cells were subsequently applied to assess their proliferation on the nanofiber. The ADSC used in the trial originated from Passage 3. This study was conducted in accordance with the standards set by the Ethics Committee of Universitas Pembangunan Nasional Veteran Jakarta (Ref. No. 8/I/2023/KEPK).

2.12. Multipotency and Differentiation Capacity Assay

This test was performed to determine the consistency of the pluripotent marker ADSC. The analysis of multipotency stem cell surface marker proteins was performed using a BD Stemflow™ hMSC (human Mesenchymal Stem Cell) Analysis Kit (BD Biosciences) on a flow cytometer. The expression of the multipotent mesenchymal stem cell markers $CD73^+$, $CD90^+$, $CD105^+$, $CD44^+$, and $CD34^-/CD45^-/CD11b^-/CD19^-$ stem cell surface marker proteins in 1×10^5 monolayer cultured ADSCs at passage 3 was incubated with a stem cell surface protein antibody for 30 min and washed with running buffer. The sample was then centrifuged at 1,200 rpm for 5 min and diluted in Phosphate-buffered saline (Gibco, USA) with 20% Fetal Bovine Serum.

Differentiation capacity assays ADSCs at passage 3 (1×10^5 cells) were performed and cultured on 24-well plates with chondrogenesis, osteogenesis, and adipogenesis medium (StemPro differentiation kit, Gibco) without a nanofiber scaffold. Cells were analyzed for GAG deposition for chondrogenesis using alcian blue, Ca^{2+} mineralization for osteogenesis using alizarin red, and intracellular lipid droplets on day 14 for adipogenesis using oil red O. The cells were subsequently washed with phosphate-buffered saline (PBS) and fixed with 4% paraformaldehyde for a period of 30 min at room temperature. Subsequently, the 4% paraformaldehyde was removed, and the reagent was added to the fixed cells for 30 min. The cells were washed three times with Millipore water for 2 min. After drying, the stained samples were observed under a light microscope, and images were captured (Rosadi *et al.* 2019). The process of differentiation with the addition of a scaffold is confirmed by detecting the expression of the biomarker genes chondrogenesis (Collagen Type II).

2.13. Cell Viability Assay

Cell viability was assessed using the CellTiter 96® AQueous One Solution Reagent containing MTS

(3-(4,5-dimethylthiazol-2-yl)-5-(3-carboxymethoxyphenyl)-2-(4-sulfophenyl)-2H-tetrazolium) (Promega, USA). ADSCs were seeded onto scaffolds composed of P(3HB-co-3HHx) and silk fibroin at ratios of 4:0, 3:1, 1:1, 1:3, and 0:4 in 24-well plates, at a density of 50,000 cells/well in 1 mL medium. Nanofibers were placed into the wells using forceps, sterilized by 30 minutes of UV exposure followed by 30 minutes in absolute ethanol. Teflon rings were autoclaved and positioned on top of the nanofibers in 12-well plates to keep them in place during culture. The cell viability assay was performed on days 3, 5, and 7. The working solution was prepared by mixing 100 µL of MTS reagent with 1 mL of DMEM low-glucose medium. After a two-hour incubation, absorbance was measured at 492 nm using a 96-well microplate reader (EZ Reader).

2.14. Total RNA Isolation and cDNA Synthesis

Cells that have been grown on scaffolds are differentiated into chondogenesis using a specific differentiation medium (StemPro differentiation kit, Gibco). Cells are collected using the methods of trypsinization and centrifugation to obtain cell pellets. Total RNA was extracted from the cell pellet using a Zymo Quick-RNA Miniprep Plus Kit. The RNA yield and concentration after extraction were determined using a NanoDrop microvolume spectrophotometer (Thermo Scientific™). cDNA synthesis was performed using ReverTraAce® qPCR RT Master Mix with gDNA Remover (Toyobo, Japan).

2.15. Quantitative Real-Time Polymerase Chain Reaction

The Primers for the housekeeping gene Collagen Type II and GAPDH (glyceraldehyde-3-phosphate dehydrogenase) were generated from Invitrogen using the sequence from the reference (Guillot 2014; Rosadi 2019) at annealing temperature of 62°C (Supplementary Table 1). RT-qPCR analysis was performed on a Real-Time Quantitative Thermal Cycler MA-6000 (Sansure) using kits from the THUNDERBIRD™ Next SYBR® qPCR Mix (Toyobo, Japan). qPCR was initiated with 1-cycle denaturation at 95°C for 30 s, followed by 50 cycles of denaturation at 95°C for 15 s and extension at 60°C for 30 s. The Melting curve analysis was performed at 94°C for 30 s, 60°C for 1 min, followed by 94°C. For each cDNA sample, triplicate analyses were performed, in which the rate of target transcription was normalized to that of GAPDH as a housekeeping gene.

2.16. Statistical Analysis

All statistical analyses were conducted using the IBM SPSS Statistics 26 software. A simple analysis of variance (ANOVA) and a post hoc Tukey's test were employed to examine differences between groups. For non-normal and non-homogeneous data, a non-parametric Kruskal-Wallis test was performed. Statistical significance was set at $p<0.05$.

3. Results

The nanofiber produced from P(3HB-co-3HH_x), P(3HB-co-3HH_x)/silk fibroin, and silk fibroin, which are the subject of this study, are presented in Figure 2. The voltage condition showed that 16,000 volts is prominent for producing nanofibers with a small diameter. Scanning electron microscopy (SEM) analysis indicated that the nanofiber possessed a porous structure with a random distribution of fibers. The fibers produced under the specified electrospinning conditions had an average diameter of 370-600 nm. The average diameter of the nanofibers decreased with an increase in the proportion of silk fibroin in the formulation (the average diameter of 0:4 ratio is 373±7 nm). Furthermore, it was observed that the distribution of fiber diameters narrowed with increasing silk fibroin content. These findings support the hypothesis that silk fibroin can be used as a control parameter to alter the average fiber diameter in nanofiber scaffolds.

The presence of silk fibroin and P(3HB-co-3HHx) was confirmed by FTIR analysis. Both 3HB and 3HHx showed a clear absorption band at 1,721 cm^{-1}, which corresponded to the carbonyl ester functional group (C=O). On the other hand, amide I and amide II

Table 1. Tensile analysis of electrospun P(3HB-co-3HHx)/silk fibroin nanofibers before and after ethanol preparation

P(3HB-co-3HHx)/silk ratio	Tensile strength (Pa)		Tensile strain (%)		Modulus young (Pa)	
	Before	After	Before	After	Before	After
4:0	0.523±0.028^{ab}	0.737±0.037^{a}	8.6±0.4^{a}	13.3±0.8^{a}	6.040±0.061^{a}	5.498±0.055^{a}
3:1	0.583±0.019^{ab}	0.532±0.016^{bc}	23.7±1.3^{bc}	31.7±1.6^{bc}	2.435±0.604^{bc}	2.198±0.859^{a}
1:1	0.330±0.191^{c}	0.486±0.111^{bc}	26.1±0.2^{bc}	28.3±1.8^{bc}	1.263±0.031^{bc}	1.708±0.061^{a}

Results are presented as mean ± standard deviation (n = 3). Mean values that different letters are significantly different (Tukey test, $p<0.05$)
The same lowercase letter indicates that there is no statistically significant difference

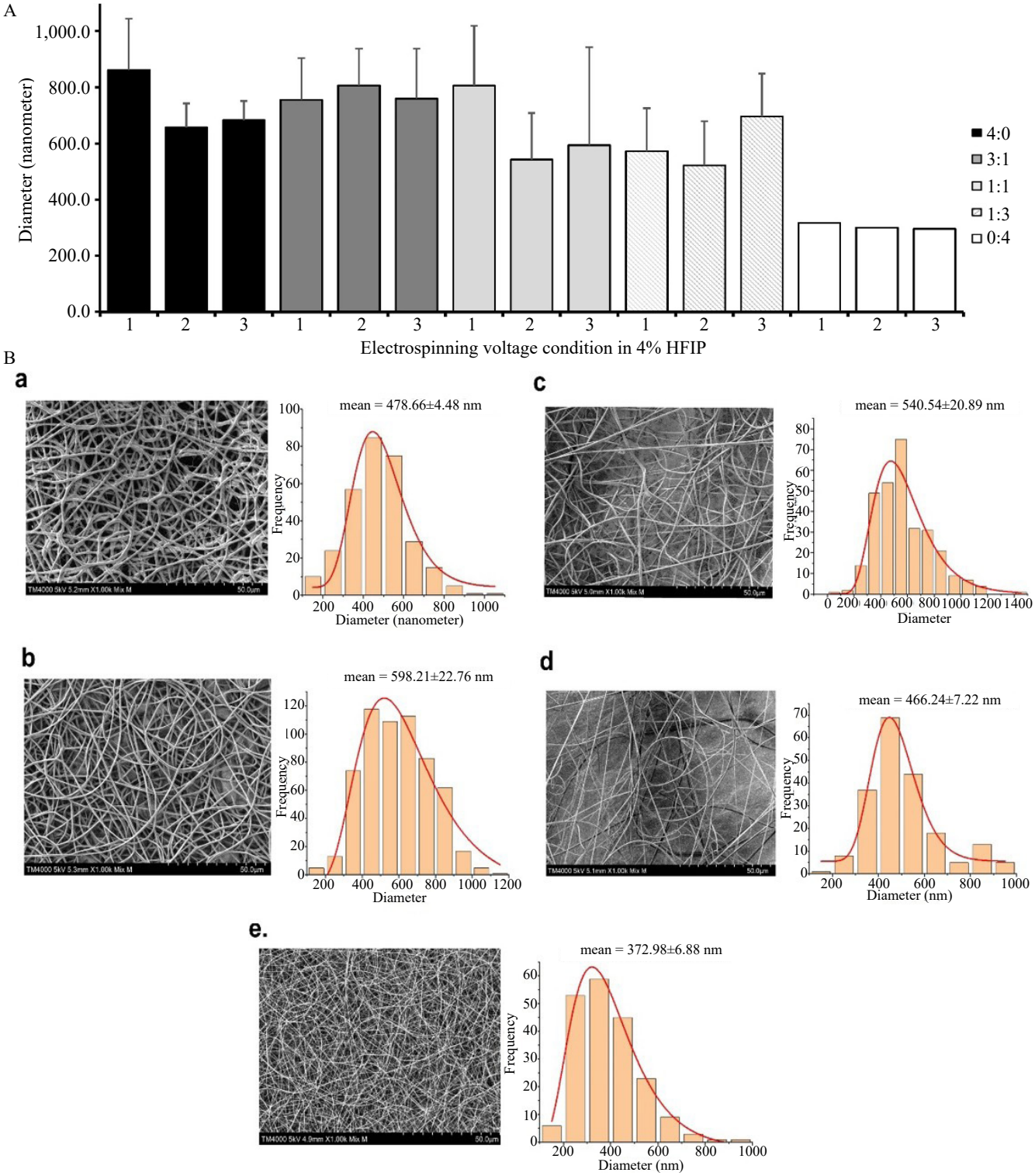

Figure 2. (A) Electrospinning voltage condition 1. 14,000 volt, 2. 16,000 volt, 3. 18,000 volt. (B) SEM photographs and the diameter distribution of the fabricated nanofiber in 16,000 volts with different ratios (a) P(3HB-co-3HHx) (b) P(3HB-co-3HHx)/silk fibroin in a ratio of 3:1. (c) P(3HB-co-3HHx)/silk fibroin in a 1:1 ratio. (d) P(3HB-co-3HHx)/silk fibroin in a 1:3 ratio (e) silk fibroin only. The image has a magnification of 1000×, and the scale bar corresponds to a length of 50 micrometers

functional groups help identify silk fibroin. The results show that the peak at 1,646 cm^{-1} is caused by the random helical structure and the C=O stretch vibration in the amide group I. In addition, the peak at 1,528 cm^{-1} is caused by the NH bending vibration of the amide II. The relative intensity of the band shows the ratio of Silk Fibroin to PHA. When the number of silk fibroin in the mixture increased, which was shown by an increase in the intensity of the characteristic bands of silk fibroin at 1,646 cm^{-1} and 1,528 cm^{-1} (Figure 3A), the intensity of the 1,721 cm^{-1} band, associated with P(3HB-co-3HHx), decreased.

The physicochemical properties of silk fibroin can affect the structure of random coils/silk I in silk fibroin, leading to the dissolution of the silk fibroin nanofiber. Swelling and destruction of silk fibroin can result from contact with water so that water molecules penetrate the amorphous region and weaken the hydrogen bonds inside the silk fibroin. Silk fibroin can transform from a random coil state to a β-sheet structure through treatment with organic solvents, such as methanol or ethanol. In this study, silk fibroin nanofibers are treated with absolute ethanol. The conformational transition before and after the ethanol preparation of silk fibroin nanofibers was analyzed by FT-IR spectroscopy, focusing on the amide regions I and II. Electrospun silk fibroin membranes show random coil conformations prior to ethanol treatment, with absorption bands at 1,646 cm^{-1} (amide I) and 1,528 cm^{-1} (amide II) (Figure 3B). The shift indicating the transition to conformation into β sheets was seen in the 1,623 cm^{-1} and 1,513 cm^{-1} band shifts, respectively (Figure 4B), after 30 minutes of ethanol treatment.

The water contact angle depends on the hydrophilicity of the surface, which is a critical factor influencing cell adhesion and proliferation. An increase in the proportion of silk fibroin in the blends reduced the water contact angle of the nanofiber. The evidence indicates that the nanofiber of P(3HBco-3HHx)/silk fibroin blended fibers exhibit increased hydrophilicity with an increase in the inclusion of silk fibroin. A water contact angle of less than 90° is indicative of hydrophilic properties. Therefore, the P(3HB-co-3HHx)/silk fibroin nanofibers, which contain a minimum of 50% silk fibroin by weight, exhibit hydrophilic properties. The water contact angle for the electrospun P(3HB-co-3HHx)/silk fibroin (3:1) membrane was determined to be 68.67±5.5°, which closely approximates that of TCPS (Tissue Culture Polystirene) plates previously optimized for cell attachment (Figure 4 and Supplementary Table 2).

The roughness results indicate that P(3HB-co-3HHx)/silk fibroin nanofibers are approximately 7.3 times more than that of P(3HB-co-3HHx) nanofibers (Supplementary Table 3). The dominance of P(3HB-co-3HHx) in the mixture had a direct impact on the roughness of the P(3HB-co-3HHx)/silk fibroin blend nanofibers, irrespective of the amount of P(3HB-co-3HHx) supplied to the mixture. Silk fibroin nanofibers exhibited significantly greater smoothness than the P(3HB-co-3HHx) membranes. The analysis revealed that the targeted inclusion of P(3HB-co-3HHx) in P(3HB-co-3HHx)/silk fibroin nanofibers increased the surface roughness, whereas silk fibroin led to a smoother biomaterial.

Tensile tests were conducted on the nanofiber to determine its mechanical properties before and after

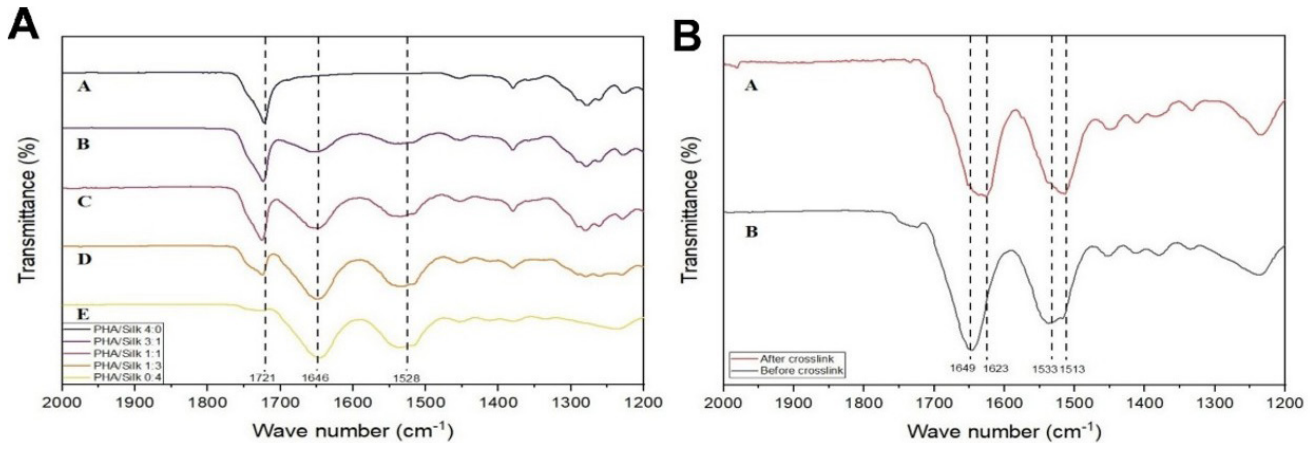

Figure 3. (A) FTIR spectra of the nanofiber, (B) FTIR spectroscopic analysis of the silk fibroin nanofiber before and after ethanol preparation. a) Before ethanol preparation b) After ethanol preparation

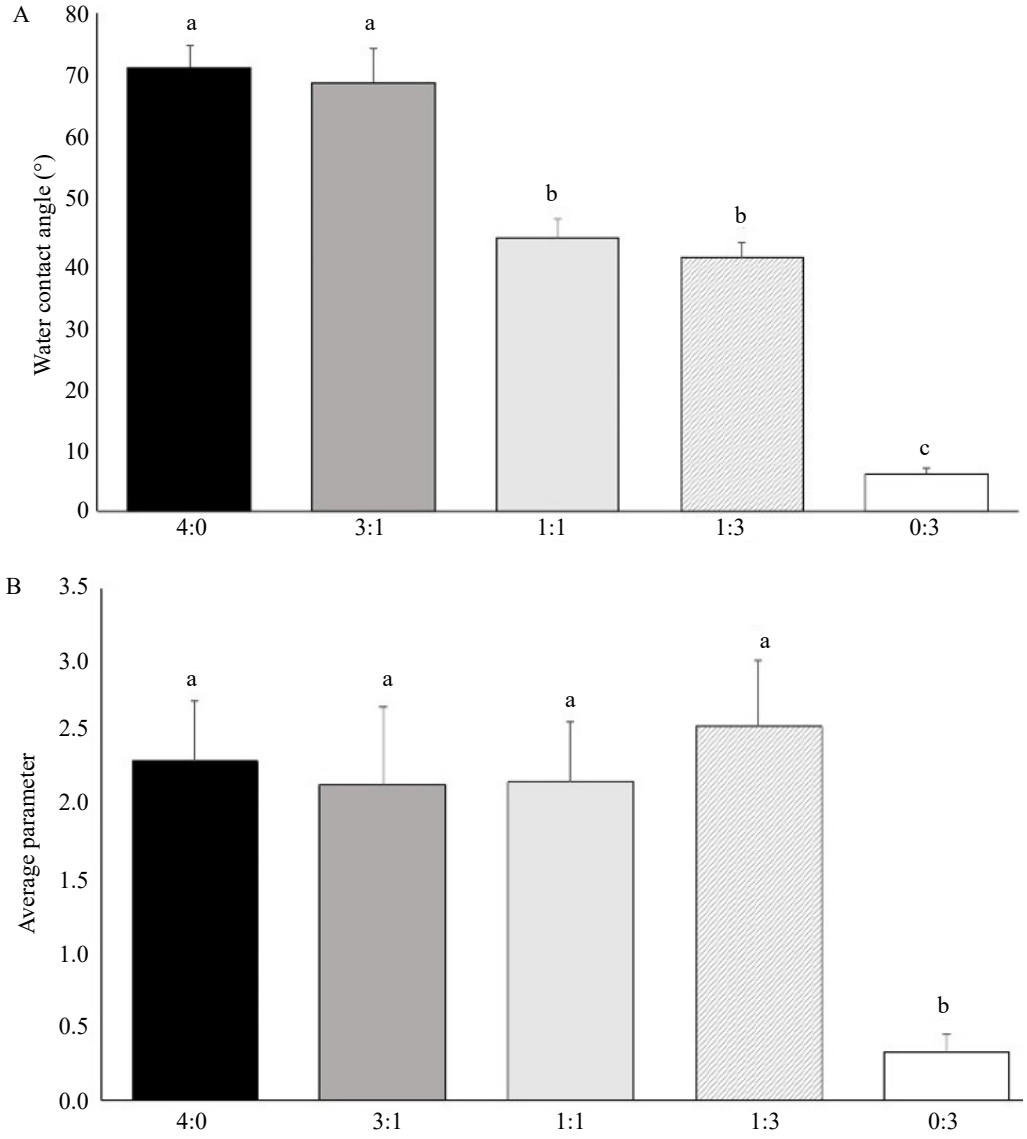

Figure 4. (A) Surface hydrophilicity of nanofiber, (B) roughness analysis of nanofiber. Significantly different mean values are indicated by different letters (Tukey test, $p<0.05$). The same lowercase letter indicates that the differences observed are not statistically significant. The results are presented as the mean ± standard deviation, with a sample size of n = 3

ethanol preparation at various P(3HB-co-3HHx)/silk fibroin ratios. Analyzing nanofibers with ratios of 1:3 and 0:4 was difficult because of the higher silk fibroin content, making them prone to tearing and unsuitable for analysis. However, the mechanical properties of the nanofiber were effectively demonstrated at P(3HB-co-3HHx)/silk fibroin ratios of 4:0, 3:1, and 1:1 (Table 1). As expected, ethanol preparation enhanced the tensile strength and tensile strain of P(3HB-co-3HHx)/silk fibroin membranes. The highest tensile strength of 0.737±0.037 Pa was attained with a 4:0 ratio after ethanol preparation, whereas the highest tensile strain of 31.7±1.6% was achieved with a 3:1 ratio after ethanol preparation. This improvement in tensile strength after ethanol preparation might be due to the interaction between the predominant carboxyl groups in P(3HB-co-3HHx). In addition, hydrogen-bonding interactions between the carboxyl functional groups of P(3HB-co-3HHx) and the amide functional group of silk fibroin resulted in a more effective stress transfer, thereby increasing the tensile strain. This suggests that the tensile strain on the membrane of P(3HB-co-3HHx)/silk fibroin can be enhanced by the addition of silk fibroin, which can increase the Young's Modulus, making it ideal for artificial tissues in biomedicine that require good energy absorption and flexibility.

The multipotent capacity of ADSC to differentiate into adipocytes, chondrocytes, and osteocytes was analyzed. ADSC was induced using a commercial induction medium. Differentiated ADSC showed intracellular lipid droplets. Cell differentiation towards osteogenesis was detected by calcium deposition using Alizarin staining. Alcian blue staining (Supplementary Figure 1) showed the formation of colored micro masses during the differentiation of ADSCs toward chondrogenesis. In addition, flow cytometric analysis was performed prior to differentiation to detect the surface marker proteins CD73 (96.034%), CD90 (95.438%), CD105 (84.976%), and CD44 (96.702%). The expression of CD34/CD45/CD11b/CD19 was negative, with less than 3% expression (Figure 9E). These results indicate that the ADSC used in this experiment met the International Society for Cellular Therapy (ISCT) criteria for adipose-derived stem cells (ADSCs).

The results of the ADSC viability analysis with P(3HB-co-3HHx), P(3HB-co-3HHx)/silk fibroin, and silk fibroin membrane showed that the number of cells on day 5 was slightly lower than on day 3 (Figure 5). This result can be attributed to the fact that ADSC requires time to integrate with biomaterials and proliferate. Cell adhesion and dissemination are components of the initial phase of cell-material interactions, and the quality of this adhesion determines the cell's ability to differentiate and proliferate. The incorporation of silk fibroin into P(3HB-co-3HHx) resulted in cell growth, suggesting that cell proliferation was facilitated. The nanofiber did not exhibit cytotoxic effects on ADSC, as evidenced by the increased proliferation rate of the ADSC. On day 7, the viability data showed that the silk fibroin electrospun membrane [P(3HB-co-3HHx)/silk fibroin ratio of 0:4 was the most effective in inducing ADSC cell proliferation, with a rate of 99.1%, implying that silk fibroin nanofiber

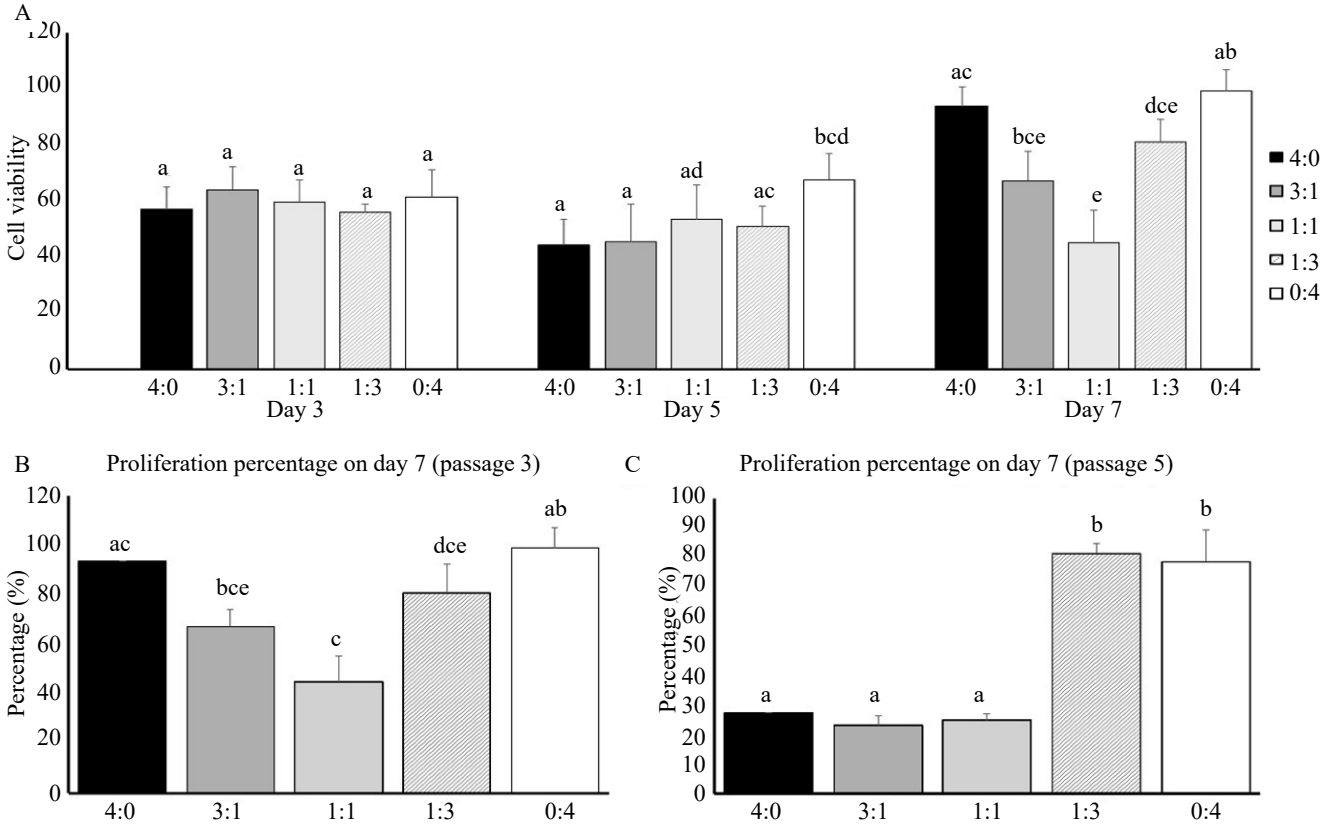

Figure 5. (A) The cell proliferation percentage of the ADSCs on the electrospun P(3HB-co-3HHx)/silk fibroin membranes with varying ratios on day 3, day 5, and day 7 at passage 3, as determined by the MTS assay. The results show that the percentage of cell proliferation of the ADSCs on the electrospun P(3HB-co-3HHx)/silk fibroin membranes with different ratios significantly increases on day 7 at different passages. ADSC was seeded to nanofibers only when they reached passages 3 and 5, and cultured for 7 days on nanofibers, (B) on day 7, the proliferation percentage was measured using the MTS assay in the third passage, (C) proliferation percentage at day 7 for passage 6 measured by MTS assay. Results are expressed as mean ± standard deviation (n = 3). Significant differences were detected (Tukey test, $p \leq 0.05$). The same lowercase letter indicates that there is no statistically significant difference

scaffolds can effectively stimulate ADSC proliferation. Moreover, the diminished cell proliferation capability was observed at higher passage numbers (passage 5). On the other hand, the cell proliferation capacity can be maintained by the addition of silk fibroin, even at increasing the cell number (Figure 5B and C), suggesting that silk fibroin may be a more suitable material for maintaining ADSC proliferation.

The results of the chondrogenesis gene expression analysis demonstrated that the incorporation of silk fibroin into nanofibers enhanced the expression of the chondrogenic biomarker of collagen type 2, reaching a value of 8.718 compared to the control, which exhibited a value of 0.00082 (Figure 6).

4. Discussion

Nanofibers consisting of P(3HB-co-3HHx), silk fibroin, and their combinations were produced using electrospinning. The incorporation of silk fibroin was shown to result in a reduction in fiber diameter, a crucial characteristic in tissue engineering scaffolds because it affects the surface area-to-volume ratio, which is a central aspect of scaffold performance (Chen *et al.* 2022). The diameter of the fiber is mostly influenced by the polymer content and parameters of the electrospinning process, which include the applied voltage, polymer concentration, needle diameter, collector distance, and extrusion rate (Angelova *et al.* 2022; Ma *et al.* 2023). It should be emphasized that the diameters shown in this study were based on the manipulation of the applied voltage, which is consistent.

Integrating silk fibroin into the P(3HB-co-3HHx) matrix enhanced the hydrophilic nature of the nanofiber. The observed phenomenon is ascribed to the enhancement of the hydrogen bonding strength between the water molecules and the polymer composite. This adhesive activity is facilitated by the amide structure and polar side chains of the amino acids serine, tyrosine, glutamic acid, and aspartic acid in silk fibroin. Consequently, there was a significant increase in both surface roughness and hydrophilicity (Selatile *et al.* 2018; Satchanska *et al.* 2024). Empirical studies have shown the crucial significance of surface hydrophilicity in facilitating cell adhesion by enhancing serum protein adsorption from the surrounding medium. Consequently, this enhances the capacity of cells to adhere to the scaffold, thereby facilitating cell adhesion and proliferation (Jeong *et al.* 2019; Hasan and Pandey 2021).

The interaction between ADSC and nanofiber is largely determined by nonspecific interactions, with the physicochemical properties and topography of the nanofiber having the greatest influence. A previous study has demonstrated that the adsorption of fibronectin on hydrophilic surfaces promotes the conformation of fibronectin, which is more conducive to cell adhesion

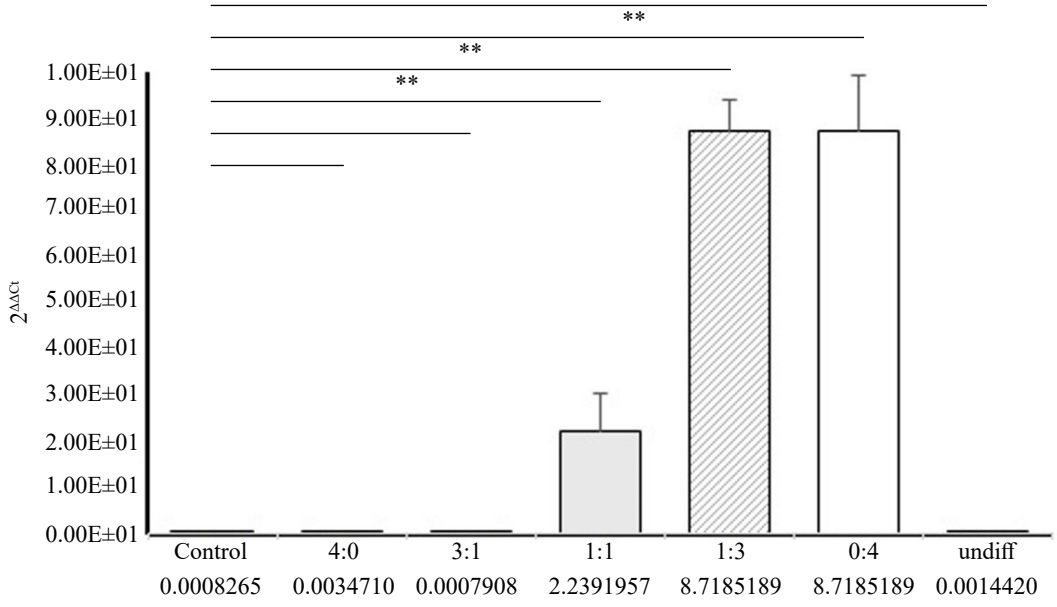

Figure 6. Collagen type II (Chondrogenesis biomarker) fold change. Control is ADSC differentiated culture without a nanofiber for 2 weeks. Undifferentiated cells (undiff) are ADSCs that are not differentiated and are taken from passages 3 ADSC cultures. The mean ± standard deviation represents the results (n=3) (Tukey test, * $p<0.05$, ** $p<0.01$)

(Kowalczyńiska *et al.* 2005). The addition of silk fibroin decreases the water contact angles and makes the nanofibers more hydrophilic (supplementary Figure 2). Furthermore, fibronectin and vitronectin adsorb more readily on hydrophilic surfaces, which in turn supports better cell adhesion and spreading in the presence of serum proteins (Arima and Iwata 2015). Another study demonstrated that silk fibroin, when combined with fibronectin, significantly improves cell attachment and viability without compromising the mechanical integrity of the fibers (Gobin *et al.* 2005; Jacobsen *et al.* 2017). Cells adhere better to smoother surfaces because of their reduced irregularity, allowing integrins to form stronger and more consistent focal adhesions. Uniformity of the biomaterial surface is crucial for promoting well-developed focal adhesions and stress fibers, which are crucial for stable cell attachment (Van Kooten *et al.* 2004; Ahn *et al.* 2014).

Silk fibroin has remarkable mechanical properties, such as elasticity, which provide both robustness and flexibility. Therefore, this could be a promising option for developing medical devices and scaffolds to promote cell proliferation and differentiation (Han *et al.* 2023). It can be assumed that the hydrophilicity and surface energy of the nanofiber influence the amount and type of adsorbed serum proteins and their conformational state on the membrane surface. This has a direct effect on cell adhesion. Optimization of these properties could lead to increased adsorption of serum proteins, which, in turn, could facilitate ADSC adhesion (Han *et al.* 2023). It should be noted that the integrins of cells can recognize the RGD sequence of these proteins. Notably, the basic amino acids in silk fibroin, particularly arginine and lysine, also play important roles in cell adhesion. These positively charged residues, which are located near the carboxy-terminal, non-repetitive region, could enter electrostatic interactions with cells and thus further support adhesion (Nasimi Shad and Moghbeli 2024). Moreover, hMSCs are mechanosensitive, which is why fibroin in silk is essential for binding extracellular matrix proteins such as fibronectin, vitronectin, and laminin. These factors are essential for cell adhesion. Fibroin also contains various functional groups, including amine, carboxyl, and hydroxyl groups. These properties enable excellent interactions with cell surfaces and adhesion proteins, which in turn significantly promote cell adhesion (Zheng and Zuo 2021).

The electrospinning technique significantly improved cell proliferation of ADSC on nanofiber P(3HB-co-3HHx)/silk fibroin nanofibers. Irregularities in the surface and topography were effectively corrected (Esmail *et al.* 2021; Sarıkaya and Gümüşderelioğlu 2021; Nasimi Shad and Moghbeli 2024). This finding directly contradicts the results of Ang *et al.* who demonstrated that the addition of silk alone to the nanofiber does not significantly improve cell viability. This discrepancy is a result of the higher silk fibroin content in the Japanese hybrid cocoon used in this study than in the cocoon used in Shaik Ling's study. A higher concentration of silk fibroin in scaffold biomaterials undoubtedly promotes cell viability. Taddei *et al.* showed that incorporating *Bombyx mori* silk fibroin into poly(L-lactic acid) nanofibers improves cell adhesion and proliferation (Taddei *et al.* 2017).

The physicochemical properties of biomaterials can induce cellular behaviors, including adhesion, proliferation, and differentiation (Bacakova *et al.* 2011). These findings indicate that the incorporation of silk fibroin into nanofibers has the potential to enhance chondrogenic differentiation. These results demonstrate that silk fibroin nanofiber properties are conducive to the differentiation of chondrogenesis, as evidenced by an increase in the expression of the type 2 collagen gene. This phenomenon can be attributed to the release of extrinsic signals into the chondrogenic differentiation medium (Chawla *et al.* 2021). This culture on nanofiber provides an environment conducive to stem cell attachment, proliferation, and chondrogenesis differentiation. Moreover, silk fibroin nanofiber scaffolds demonstrated strong potential for cartilage tissue engineering by enhancing chondrogenic differentiation. Future studies should focus on validating their performance in 3D culture and *in vivo* models to establish clinical applicability.

In conclusion, the addition of silk fibroin improves the scaffold's hydrophilicity, mechanical strength, and physicochemical properties, thereby supporting better proliferation and differentiation of ADSCs. This study highlights that the physicochemical properties of the nanofiber composite play a crucial role in regulating the growth and differentiation of human adipose-derived mesenchymal stem cells. Experimental findings further revealed that silk fibroin promotes chondrogenesis and shows strong potential for modulating chondrogenesis differentiation markers.

Conflict of Interest

The authors declare no conflict of interest.

Funding

This research was supported by an External Grant from Riset dan Inovasi untuk Indonesia Maju (RIIM) BRIN LPDP 2024, an Internal Grant RISTI 2022 from Universitas Pembangunan Nasional Veteran Jakarta and SAME (Scheme Academic for Mobility and Exchange) 2022 Kemendikbudristek.

Acknowledgements

The authors acknowledge the facilities and scientific and technical support from the Advanced Characterization Laboratories Cibinong, Integrated Laboratory of Bioproduct and Advanced Characterization Laboratories Serpong, National Research and Innovation Agency through E-Layanan Sains, Badan Riset, and Inovasi Nasional.

References

Ahn, H.H., Lee, I.W., Lee, H.B., Kim, M.S., 2014. Cellular behavior of human adipose-derived stem cells on wettable gradient polyethylene surfaces. *International Journal of Molecular Sciences.* 15, 2075-2086. https://doi.org/10.3390/ijms15022075

Ang, S.L., Shaharuddin, B., Chuah, J.A., Sudesh, K., 2020. Electrospun poly(3-hydroxybutyrate-co-3-hydroxyhexanoate)/silk fibroin film is a promising scaffold for bone tissue engineering. *International Journal of Biological Macromolecules*. 145, 173-188. https://doi.org/10.1016/j.ijbiomac.2019.12.149

Angelova, L., Daskalova, A., Filipov, E., Vila, X.M., Tomasch, J., Avdeev, G., Teuschl-Woller, A.H., Buchvarov, I., 2022. Optimizing the surface structural and morphological properties of silk thin films via ultra-short laser texturing for creation of muscle cell matrix model. *Polymers.* 14, 2584. https://doi.org/10.3390/polym14132584

Arima, Y., Iwata, H., 2015. Preferential adsorption of cell adhesive proteins from complex media on self-assembled monolayers and its effect on subsequent cell adhesion. *Acta Biomaterialia*. 26, 72-81. https://doi.org/10.1016/j.actbio.2015.08.033

Bacakova, L., Filova, E., Parizek, M., Ruml, T., Svorcik, V., 2011. Modulation of cell adhesion, proliferation and differentiation on materials designed for body implants. *Biotechnol. Adv*. 29, 739-767. https://doi.org/10.1016/j.biotechadv.2011.06.004

Barcena, A.J.R., Mishra, A., Bolinas, D.K.M., Martin, B.M., Melancon, M.P., 2024. Integration of electrospun scaffolds and biological polymers for enhancing the delivery and efficacy of mesenchymal stem/stromal cell therapies. *Front Biosci.* 29, 228. https://doi.org/10.31083/j.fbl2906228

Bari, E., Scocozza, F., Perteghella, S., Sorlini, M., Auricchio, F., Torre, M.L., Conti, M., 2021. 3d bioprinted scaffolds containing mesenchymal stem/stromal lyosecretome: next generation controlled release device for bone regenerative medicine. *Pharmaceutics.* 13, 515. https://doi.org/10.3390/pharmaceutics13040515

Chawla, S., Desando, G., Gabusi, E., Sharma, A., Trucco, D., Chakraborty, J., Manferdini, C., Petretta, M., Lisignoli, G., Ghosh, S., 2021. The effect of silk-gelatin bioink and TGF-β3 on mesenchymal stromal cells in 3D bioprinted chondrogenic constructs: a proteomic study. *Journal of Materials Research*. 36, 4051-4067. https://doi.org/10.1557/s43578-021-00230-5

Chen, Y., Dong, X., Shafiq, M., Myles, G., Radacsi, N., Mo, X., 2022. Recent advancements on three-dimensional electrospun nanofiber scaffolds for tissue engineering. *Adv. Fiber Mater.* 4, 959–986. https://doi.org/10.1007/S42765-022-00170-7

Esmail, A., Pereira, J.R., Zoio, P., Silvestre, S., Menda, U.D., Sevrin, C., Grandfils, C., Fortunato, E., Reis, M.A.M., Henriques, C., Oliva, A., Freitas, F., 2021. Oxygen plasma treated-electrospun polyhydroxyalkanoate scaffolds for hydrophilicity improvement and cell adhesion. *Polymers.* 13, 1056. https://doi.org/10.3390/polym13071056

Gobin, A.S., Froude, V.E., Mathur, A.B., 2005. Structural and mechanical characteristics of silk fibroin and chitosan blend scaffolds for tissue regeneration. *Journal of Biomedical Materials Research.* 74A, 465-473. https://doi.org/10.1002/jbm.a.30382

Guillot, C., Favaudon, V., Herceg, Z., Sagne, C., Sauvaigo, S., Merle, P., Hall, J., Chemin, I., 2014. PARP inhibition and the radiosensitizing effects of the PARP inhibitor ABT-888 in *in vitro* hepatocellular carcinoma models. *BMC Cancer.* 14, 603. https://doi.org/10.1186/1471-2407-14-603

Han, Feng, Meng, Q., Xie, E., Li, K., Hu, J., Chen, Q., Li, J., Han, Fengxuan, 2023. Engineered biomimetic micro/nano-materials for tissue regeneration. *Front. Bioeng. Biotechnol.* 11, 1205792. https://doi.org/10.3389/fbioe.2023.1205792

Hasan, A., Pandey, L.M., 2021. Implications of the nanoscopic surface modification on the protein adsorption and cell adhesion, in: Sarma, H., Joshi, S.J., Prasad, R., Jampilek, J. (Eds.), *Biobased Nanotechnology for Green Applications. Nanotechnology in the Life Sciences.* Springer, Cham, pp. 423–460. https://doi.org/10.1007/978-3-030-61985-5_16

Jacobsen, M.M., Li, D., Gyune Rim, N., Backman, D., Smith, M.L., Wong, J.Y., 2017. Silk-fibronectin protein alloy fibres support cell adhesion and viability as a high strength, matrix fibre analogue. *Scientific Reports.* 7, 1-11. https://doi.org/10.1038/srep45653

Jeong, J., Kim, J.H., Shim, J.H., Hwang, N.S., Heo, C.Y., 2019. Bioactive calcium phosphate materials and applications in bone regeneration. *BioMed Central.* 23, 1-11. https://doi.org/10.1186/s40824-018-0149-3

Kangari, P., Talaei-Khozani, T., Razeghian-Jahromi, I., Razmkhah, M., 2020. Mesenchymal stem cells: amazing remedies for bone and cartilage defects. *Stem Cell Research & Therapy.* 2020 11:1. BioMed Central, 11, 492. https://doi.org/10.1186/s13287-020-02001-1

Kiyosawa, M., Ito, E., Shirai, K., Kanekatsu, R., Miura, M., Kiguchi, K., 1999. Cocoon spinning behavior in the silkworm, *Bombyx mori*: comparison of three strains constructing different cocoons in shape. *Zoological Society of Japan*. 16, 215-223. https://doi.org/10.2108/zsj.16.215

Kopf, S., Åkesson, D., Skrifvars, M., 2023. Textile fiber production of biopolymers-a review of spinning techniques for polyhydroxyalkanoates in biomedical applications. *Polymer Reviews. Taylor & Francis*. 63, 200-245. https://doi.org/10.1080/15583724.2022.2076693

Kowalczyńska, H.M., Nowak-Wyrzykowska, M., Kołos, R., Dobkowski, J., Kamiński, J., 2005. Fibronectin adsorption and arrangement on copolymer surfaces and their significance in cell adhesion. *Journal of Biomedical Materials Research.* 72A, 228-236. https://doi.org/10.1002/jbm.a.30238

Ma, M., Zhou, H., Gao, S., Li, N., Guo, W., Dai, Z., 2023. Analysis and prediction of electrospun nanofiber diameter based on artificial neural network. *Polymers.* 15, p. 2813. https://doi.org/10.3390/polym15132813

Murugan, P., Gan, C.Y., Sudesh, K., 2017. Biosynthesis of P(3HB-co-3HHx) with improved molecular weights from a mixture of palm olein and fructose by *Cupriavidus necator* Re2058/pCB113. *International Journal of Biological Macromolecules*. 102, 1112-1119. https://doi.org/10.1016/j.ijbiomac.2017.05.006

Nasimi Shad, A., Moghbeli, M., 2024. Integrins as the pivotal regulators of cisplatin response in tumor cells. *Cell Commun Signal.* 22, 265 https://doi.org/10.1186/s12964-024-01648-0

Pecorini, G., Braccini, S., Parrini, G., Chiellini, F., Puppi, D., 2022. Additive manufacturing of Poly(3-hydroxybutyrate-co-3-hy-droxyvalerate)/Poly(D,L-lactide-co-glycolide) biphasic scaffolds for bone tissue regeneration. *International Journal of Molecular Sciences*. 23, 3895. https://doi.org/10.3390/ijms23073895

Rockwood, D.N., Preda, R.C., Yücel, T., Wang, X., Lovett, M.L., Kaplan, D.L., 2011. Materials fabrication from *Bombyx mori* silk fibroin. *Nature Protocols.* 6, 1612-1631. https://doi.org/10.1038/nprot.2011.379

Rosadi, I., Karina, K., Rosliana, I., Sobariah, S., Afini, I., Widyastuti, T., Barlian, A., 2019. *In vitro* study of cartilage tissue engineering using human adipose-derived stem cells induced by platelet-rich plasma and cultured on silk fibroin scaffold. *Stem Cell Res Ther*. 10, 369. https://doi.org/10.1186/s13287-019-1443-2

Sarıkaya, B., Gümüşderelioğlu, M., 2021. Aligned silk fibroin/poly-3-hydroxybutyrate nanofibrous scaffolds seeded with adipose-derived stem cells for tendon tissue engineering. *International Journal of Biological Macromolecules*. 193, 276-286. https://doi.org/10.1016/j.ijbiomac.2021.10.104

Satchanska, G., Davidova, S., Petrov, P.D., 2024. Natural and synthetic polymers for biomedical and environmental applications. *Polymers.* 16, 1159. https://doi.org/10.3390/polym16081159

Selatile, K., Mural, P.K.S., Sinha Ray, S., 2018. Electrospun polymer nanocomposites. In: Sinha Ray S. (Eds.). *Processing of Polymer-based Nanocomposites. Springer Series in Materials Science, vol 278.* Cham: Springer. pp. 199–229. https://doi.org/10.1007/978-3-319-97792-8_7

Taddei, P., Tozzi, S., Zuccheri, G., Martinotti, S., Ranzato, E., Chiono, V., Carmagnola, I., Tsukada, M., 2017. Intermolecular interactions between *B. mori* silk fibroin and poly(l-lactic acid) in electrospun composite nanofibrous scaffolds. *Materials Science and Engineering: C.* 70, 777-787. https://doi.org/10.1016/j.msec.2016.09.055

Van Kooten, T.G., Spijker, H.T., Busscher, H.J., 2004. Plasma-treated polystyrene surfaces: model surfaces for studying cell-biomaterial interactions. *Biomaterials.* 25, 1735-1747. https://doi.org/10.1016/j.biomaterials.2003.08.071

Zhang, L., Zhang, W., Hu, Y., Fei, Y., Liu, H., Huang, Z., Wang, C., Ruan, D., Heng, B.C., Chen, W., Shen, W., 2021. Systematic review of silk scaffolds in musculoskeletal tissue engineering applications in the recent decade. *ACS Biomaterials Science and Engineering.* 7, 817-840. https://doi.org/10.1021/acsbiomaterials.0c01716

Zheng, H., Zuo, B., 2021. Functional silk fibroin hydrogels: preparation, properties and applications. *Journal of Materials Chemistry B.* 9, 1238-1258. https://doi.org/10.1039/D0TB02099K

Supplementary Materials

Supplementary Table 1. Primer design

Primer	Sequences	TM (°C)	Amplicon size (bp)
Collagen Type II (NM_001844.4)	F, 5′-GAACCCAGAAACAACACAATCC-3’ R, 5′-CATTCAGTGCAGAGTCCTAGAG-3′	60	64
GAPDH (NM_002046.7)	F, 5’-CAAGAGCACAAGAGGAAGAGAG-3’ R, 5’-CTACATGGCAACTGTGAGGAG-3’	60	80

Supplementary Table 2. Surface hydrophilicity of nanofiber

Sample	Water Contact Angle (°)	Representative image
P(3HB-co-3HHX)	71±3.6[a]	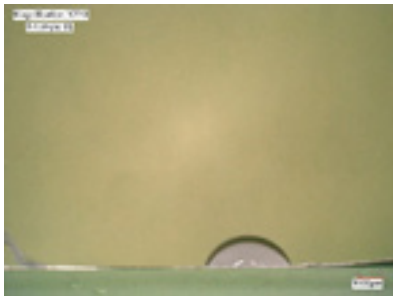
P(3HB-co-3HHX)/SF 3:1	68.67±5.5[a]	
P(3HB-co-3HHX)/SF 1:1	43.67±3.21[b]	

Significantly different mean values are indicated by different letters (Tukey test, $p<0.05$). The same lowercase letter indicates that the differences observed are not statistically significant. The results are presented as the mean from triplicate experiment

Supplementary Table 2. Continued

Sample	Water Contact Angle (°)	Representative image
P(3HB-co-3HHX)/SF 1:3	40.67±2.51[b]	
SF	6±1[c]	
Tissue culture polystirene	60-68	

Significantly different mean values are indicated by different letters (Tukey test, $p<0.05$). The same lowercase letter indicates that the differences observed are not statistically significant. The results are presented as the mean from triplicate experiment

Supplementary Table 3. Roughness analysis of Nanofiber

Sample	Average parameter	Representative image	Representative image
P(3HB-co-3HHX)	Ra: 2.32±0.41[a]		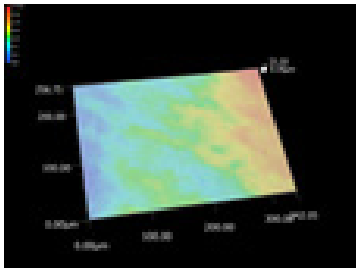
P(3HB-co-3HHX)/SF 3:1	Ra: 2.16±0.53[a]	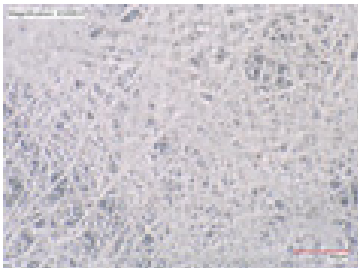	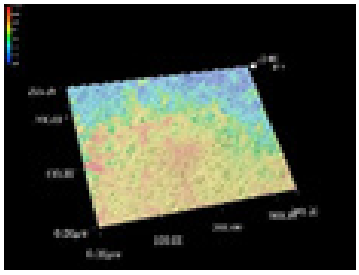

The resuls are given as the mean from triplicate analysis. The means labelled with different letters are significantly different (Tukey test, $p<0.05$). The same lowercase letter indicates that there is no statistically significant difference

Supplementary Table 3. Continued

Sample	Average parameter	Representative image	Representative image
P(3HB-co-3HHX)/SF 1:1	Ra: 2.18±0.41[a]		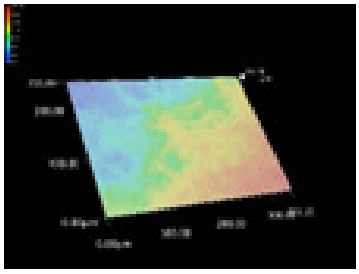
P(3HB-co-3HHX)/SF 1:3	Ra: 2.56±0.45[a]		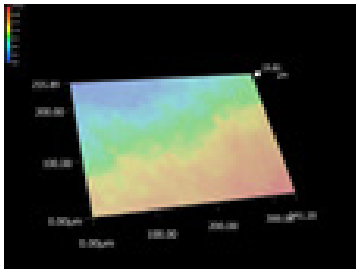
SF	Ra: 0.33±0.125[b]	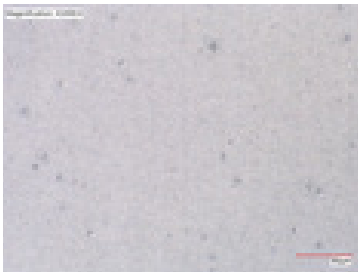	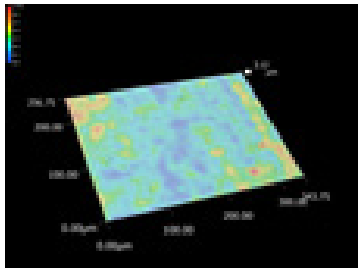

The resuls are given as the mean from triplicate analysis. The means labelled with different letters are significantly different (Tukey test, $p<0.05$). The same lowercase letter indicates that there is no statistically significant difference

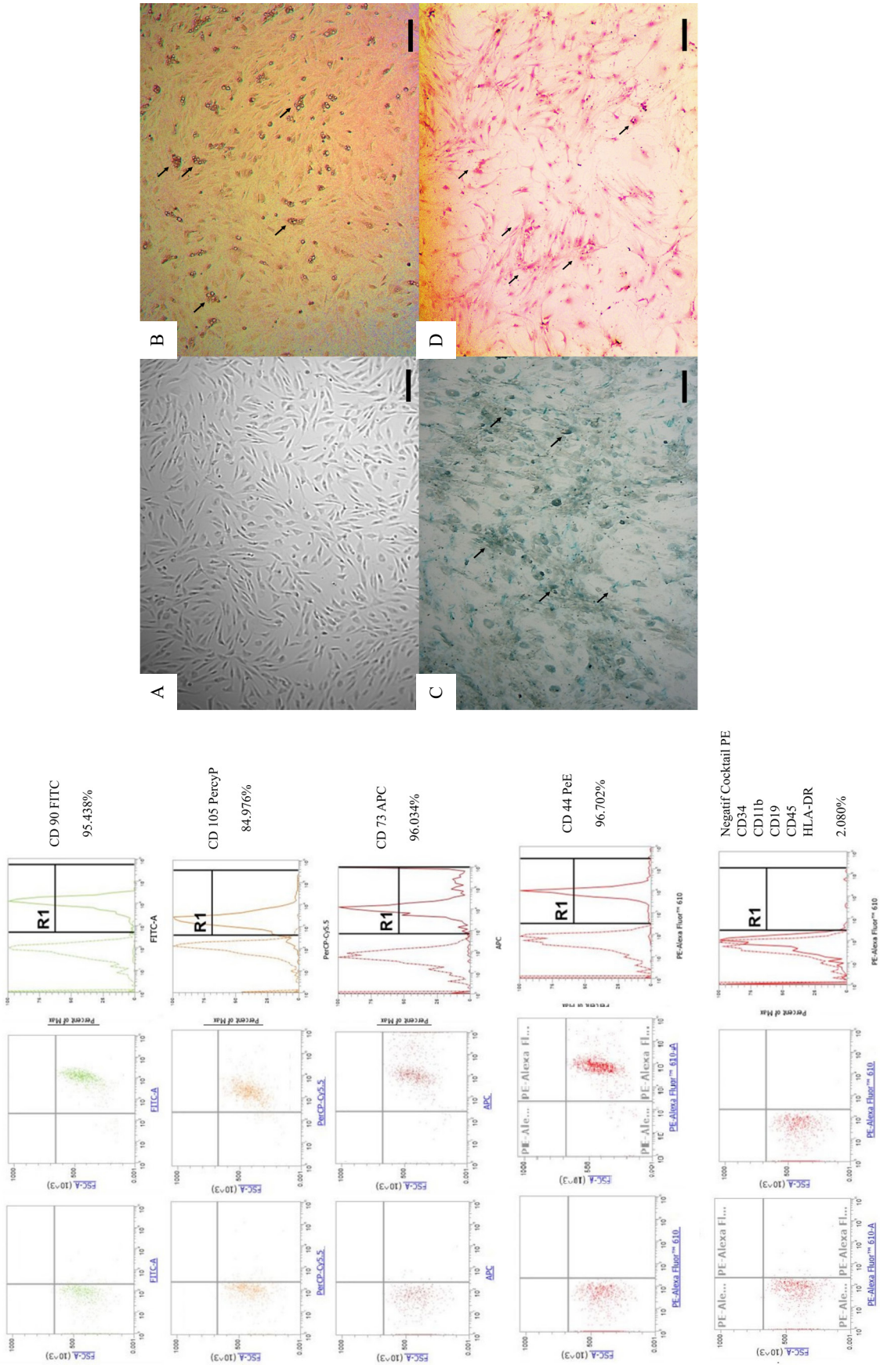

Supplementary Figure 1. Characterization of undifferentiated ADSC and differentiation capacity. Magnification of 40X. a Isolated cells from adipose tissue at passage 3 day 3 showed fibroblast-like morphology (A) multipotency of cells at passage 3 isolated from adipose tissue: differentiation into adipocytes characterized by lipid droplets (black arrows) using Oil Red O staining (B) osteocytes characterized by calcium deposits (black arrow) using alizarin red staining (C) chondrocytes formed micromass-like structures (D) using alcian blue staining (black arrow) (black bar = 50 µm) Optilab Microscope, Nikon; Cells at passage 3 expresses CD90 (99.438%), CD105 (84.976%), CD73 (96.034%) and CD44 (96.702%) and CD45/CD34/CD11b/CD19/HLA-DR % (2.080%)